IOP PUBLISHING CLASSICAL AND QUANTUM GRAVITY

Class. Quantum Grav. **24** (2007) S491–S499 doi:10.1088/0264-9381/24/19/S12

Coincidence analysis between periodic source candidates in C6 and C7 Virgo data

F Acernese[1], P Amico[2], M Alshourbagy[3], F Antonucci[4], S Aoudia[5], P Astone[4], S Avino[1], D Babusci[6], G Ballardin[7], F Barone[1], L Barsotti[3], M Barsuglia[8], Th S Bauer[9], F Beauville[10], S Bigotta[3], S Birindelli[3], M A Bizouard[8], C Boccara[11], F Bondu[5], L Bosi[2], C Bradaschia[3], S Braccini[3], F J van den Brand[9], A Brillet[5], V Brisson[8], D Buskulic[10], E Calloni[1], E Campagna[12], F Carbognani[7], F Cavalier[8], R Cavalieri[7], G Cella[3], E Cesarini[12], E Chassande-Mottin[5], N Christensen[7], C Corda[3], A Corsi[4], F Cottone[2], A-C Clapson[8], F Cleva[5], J-P Coulon[5], E Cuoco[7], A Dari[2], V Dattilo[7], M Davier[8], M del Prete[3], R De Rosa[1], L Di Fiore[1], A Di Virgilio[3], B Dujardin[5], A Eleuteri[1], M Evans[7], I Ferrante[3], F Fidecaro[3], I Fiori[7], R Flaminio[7,10], J-D Fournier[5], S Frasca[4], F Frasconi[3], L Gammaitoni[2], F Garufi[1], E Genin[7], A Gennai[3], A Giazotto[3], G Giordano[6], L Giordano[1], R Gouaty[10], D Grosjean[10], G Guidi[12], S Hamdani[7], S Hebri[7], H Heitmann[5], P Hello[8], D Huet[7], S Karkar[10], S Kreckelbergh[8], P La Penna[7], M Laval[5], N Leroy[8], N Letendre[10], B Lopez[7], Lorenzini[12], V Loriette[11], G Losurdo[12], J-M Mackowski[13], E Majorana[4], C N Man[5], M Mantovani[3], F Marchesoni[2], F Marion[10], J Marque[7], F Martelli[12], A Masserot[10], M Mazzoni[12], L Milano[1], F Menzinger[7], C Moins[7], J Moreau[11], N Morgado[13], B Mours[10], F Nocera[7], C Palomba[4], F Paoletti[3,7], S Pardi[1], A Pasqualetti[7], R Passaquieti[3], D Passuello[3], F Piergiovanni[12], L Pinard[13], R Poggiani[3], M Punturo[2], P Puppo[4], S van der Putten[9], K Qipiani[1], P Rapagnani[4], V Reita[11], A Remillieux[13], F Ricci[4], I Ricciardi[1], P Ruggi[7], G Russo[1], S Solimeno[1], A Spallicci[5], M Tarallo[3], M Tonelli[3], A Toncelli[3], E Tournefier[10], F Travasso[2], C Tremola[3], G Vajente[3], D Verkindt[10], F Vetrano[12], A Viceré[12], J-Y Vinet[5], H Vocca[2] and M Yvert[10]

[1] INFN, sezione di Napoli and/or Università di Napoli 'Federico II' Complesso Universitario di Monte S Angelo, and/or Università di Salerno, Fisciano (Sa), Italy
[2] INFN, Sezione di Perugia and/or Università di Perugia, Perugia, Italy
[3] INFN, Sezione di Pisa and/or Università di Pisa, Pisa, Italy
[4] INFN, Sezione di Roma and/or Università 'La Sapienza', Roma, Italy
[5] Departement Artemis—Observatoire de la Côte d'Azur, BP 42209 06304 Nice, Cedex 4, France
[6] INFN, Laboratori Nazionali di Frascati, Frascati (Rm), Italy
[7] European Gravitational Observatory (EGO), Cascina (Pi), Italy
[8] LAL, Univ Paris-Sud, IN2P3/CNRS, Orsay, France
[9] NIKHEF, NL-1009 DB Amsterdam and/or Vrije Universiteit, NL-1081 HV Amsterdam, The Netherlands
[10] Laboratoire d'Annecy-le-Vieux de Physique des Particules (LAPP), IN2P3/CNRS, Université de Savoie, Annecy-le-Vieux, France
[11] ESPCI, Paris, France

[12] INFN, Sezione di Firenze/Urbino, Sesto Fiorentino, and/or Università di Firenze, and/or Università di Urbino, Italy
[13] LMA, Villeurbanne, Lyon, France

E-mail: cristiano.palomba@roma1.infn.it

Received 13 April 2007, in final form 29 May 2007
Published 19 September 2007
Online at stacks.iop.org/CQG/24/S491

Abstract
In this paper, we describe the analysis performed in the data of C6 and C7 commissioning runs of Virgo for the search of periodic sources of gravitational waves. The analysis is all-sky, covers the frequency range between 50 Hz and 1050 Hz and neutron star spin-down rate below 1.58×10^{-8} Hz s^{-1}. Coincidences in the source parameter space between candidates found in the two data sets are required to reduce the false alarm probability. The procedure used to estimate the detection efficiency of the analysis pipeline, through the injection of simulated signals in the data, is also described.

PACS numbers: 04.80.Nn, 07.05.Kf, 97.60.Jd

(Some figures in this article are in colour only in the electronic version)

1. Introduction

Theoretical models suggest that $\sim 10^9$ neutron stars should be present in the galaxy. Of these, only $\sim 10^5$ are expected to be pulsars. Then, it is likely that many potentially interesting sources are not visible in the electromagnetic band. An isolated neutron star emits gravitational waves if its shape deviates from axisymmetry. This deviation is measured by the ellipticity, which is likely to have a maximum possible value smaller than 10^{-6}. Neutron stars may have a large rotation rate at birth, with rotation frequency $f_{\rm rot}$ up to 1000–1500 Hz, depending on the equation of state. For a non-axisymmetric neutron star rotating around one of the principal axis of inertia the gravitational wave frequency is $f = 2f_{\rm rot}$. The signal at the detector is frequency and amplitude modulated due to the Doppler effect and detector radiation pattern, depending on the source position and wave polarization. We use ecliptical coordinates (λ, β) for the source sky position. Interferometric detectors of the first generation have a rather small 'detection horizon': for high frequency sources and assuming a reasonable ellipticity it is of the order of a few hundred parsecs. This means that the local distribution of neutron stars can play a significant role and we cannot assume that neutron stars' population is simply distributed on the galactic disc [1]. Moreover, we need to search for young sources, which are likely to rotate faster and be more deformed (larger $\dot{f}$). All this brings us to consider the fundamental importance of making a 'blind' search of periodic sources, i.e. without making a strict hypothesis on the source parameters: position (λ, β), frequency f and spin-down rate $\dot{f}$.

The blind search for periodic sources of gravitational waves cannot be performed using optimal data analysis methods due to the huge number of points in the source parameter space that should be explored [2]. We have developed a sub-optimal hierarchical procedure

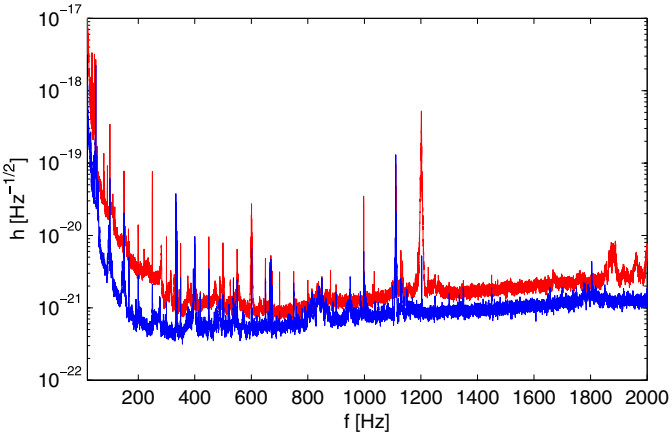

Figure 1. Noise spectral density of the Virgo data acquired during run C6 (red—light grey in the print version) and C7 (blue—dark grey in the print version) in the range [50, 2000] Hz.

that allows us to strongly reduce the needed computing power with a small reduction in sensitivity. In the following sections, we will describe the different steps of the procedure and its application to the data of Virgo commissioning runs C6 and C7. Run C6 was performed between 29 July and 12 August 2005, with an actual observation time of $T_{\rm obs} = 13.87$ days. Run C7 extended from 14 September to 19 September 2005, covering $T_{\rm obs} = 3.37$ actual days of data. In figure 1, the noise spectral densities of C6 and C7 have been plotted.

2. The analysis pipeline

The hierarchical procedure for the search of periodic sources starts from the h-reconstructed channel of two or more data sets, which could belong to a single detector or to different detectors [3]. A series of steps is applied to each data set, as briefly described in the following. More details can be found in [2, 4, 5]. See, e.g., [6] for a description of the methods used in LIGO detectors.

2.1. Removal of big time domain disturbances

A *cleaning* procedure is applied to the data, which have a sampling time $t_{\rm sampl} = 0.000\,25$ s, in order to remove big short time domain disturbances (events) which would increase the overall level of noise. First, events are identified by setting a threshold on the critical ratio $\mathrm{CR} = \frac{x_i - \mu_i}{\sigma_i}$, where x_i are the samples and μ_i and σ_i are the mean and the standard deviation computed through an autoregressive procedure. In this analysis we have set the threshold to 6. Then, events are removed setting to zero the samples corresponding to the event duration (properly defined) and using a smooth connection to the samples around it. In this way, 8109 events have been removed for C6, covering a total time of ∼1000 s (i.e. a fraction 8.3×10^{-4} of the data set), and 1963 for C7, covering ∼361 s (a fraction 1.2×10^{-3} of the data set).

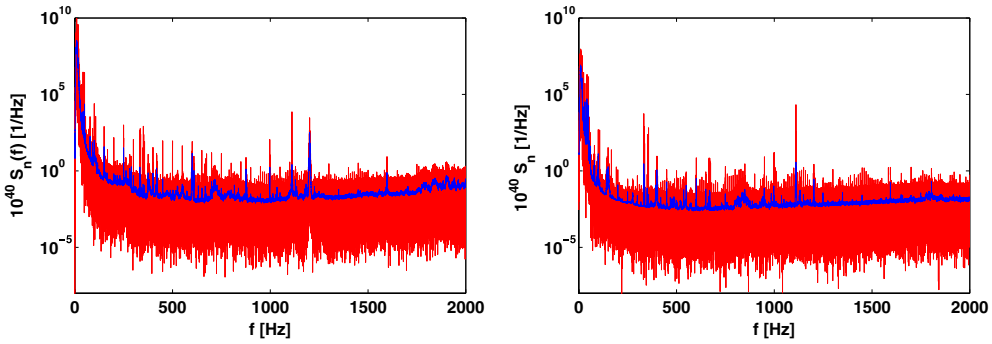

Figure 2. One spectrum, in red (light grey in the print version), and its average estimation, in blue (dark grey in the print version), for C6 (left) and C7 (right).

2.2. Construction of the short FFT database (SFDB)

Starting from the *cleaned* data, the FFTs are built with such a length that the Doppler effect and source spin-down cannot shift a frequency by more than half a bin. This implies a constraint on the maximum length of the chunks of data from which the FFT are computed, given by $T_{\mathrm{FFT,max}} = 1.1 \times 10^5/\sqrt{f}$ s where f is the frequency in Hz. In this initial analysis of real Virgo data we have used a duration $T_{\mathrm{FFT}} = 1048.576$ s at all frequencies, below the maximum allowed. The corresponding frequency bin width is $\delta f = T_{\mathrm{FFT}}^{-1} = 9.5367 \times 10^{-4}$ Hz. With this choice that, as we will see, implies a low resolution in the sky grid (especially at low frequencies), we have $N_{\mathrm{FFT}} = 2286$ FFTs for C6, and $N_{\mathrm{FFT}} = 556$ for C7. FFTs are overlapped by the half and each of them also contains a sub-sampled estimation of the spectrum, needed for a good detection efficiency in the identification of peaks (see the next point), and for the next steps of the analysis, like the adaptive Hough transform [8].

2.3. Average spectrum estimation

This estimation is done in order to not be affected by narrow spectral peaks, which could be due to gravitational signals, but to be able to follow slow or rapid variation of the noise level. For a given FFT, with samples (modulus) $\tilde{x}_i$, $i = 1, \ldots, N$ (with N being the length of the FFT), the estimator of the average $\tilde{\mu}_i$ is computed through an autoregressive procedure. For each sample, the ratio $r = \tilde{x}_i/\tilde{\mu}_{i-1}$ is computed. A threshold $V_{\max}$ ($V_{\max} = 1.58$ in this analysis) and a maximum *age* of the process $A_{\max}$ ($A_{\max} = 0.02$ Hz) are chosen; if $r < V_{\max}$ the last datum is used to evaluate the actual mean $\tilde{\mu}_i$ and the *age* A of the process is set to zero. When $r \geqslant V_{\max}$ the last datum $\tilde{x}_i$ is not used to evaluate the actual mean $\tilde{\mu}_i$ and the *age* A is incremented by δf. If the *age* A becomes larger than $A_{\max}$ we decide that the characteristics of the noise changed and we go back by $n = (A/\delta f)_{\mathrm{int}}$ samples and begin a new evaluation of the mean, restarting from the sample $i - (A/\delta f)_{\mathrm{int}}$. In figure 2, one spectrum and its estimation for C6 and C7 is plotted.

2.4. Construction of the time–frequency peak map

The time–frequency peak map is obtained making the ratio between each periodogram (square of the FFT) of the database and the corresponding estimation of the average spectrum, and selecting local maxima above a given threshold. This guarantees a high robustness against

non-stationarities. Typical values of the ratio are around 1 with significant deviations when spectral peaks are present. The threshold is chosen as a compromise between the need to minimize both the sensitivity loss and the computing power needed for the incoherent step. In this analysis we have used a threshold $\theta = 2.5$. As many disturbances are present in the data, a further *cleaning* procedure is applied at the level of the peak map by eliminating those frequencies where the peak frequency distribution is particularly high (a fraction ∼2–3% of the frequency bins is removed). In this way, we reduce the number of candidates *of the first order*[14] found with the Hough transform[15], see the next point.

2.5. Hough transform and candidate selection

The Hough transform connects the time–frequency plane to the source parameter space. The analysis presented in this paper is full-sky, covers the frequency range between 50 Hz and 1050 Hz, and spin-down rate between 0 and $\dot{f}_{\max} = 1.58 \times 10^{-8}$ Hz s^{-1}. The number of points in the source parameter space can be computed as follows. The number of frequency bins to be analysed is $N_f = 1000 \times \delta f = 1.048 \times 10^6$ for each data set. The sky resolution, which is proportional to f^{-1}, varies in both coordinates from 7.5° at 50 Hz to 0.34° at 1050 Hz. Correspondingly, the number of different locations in the sky is $N_{\rm sky} \simeq 5.06 \times 10^5$ for both data sets. The minimum spin-down age too, $\tau = f/|\dot{f}|$, is a function of the frequency and varies between 100 yr at 50 Hz and 2100 yr at 1050 Hz. The range $[0, \dot{f}_{\max}]$ is analysed in $N_{\rm sd} = 40$ steps for C6 ($\delta\dot{f} = 4.06 \times 10^{-10}$ Hz s^{-1}) and in $N_{\rm sd} = 10$ steps for C7 ($\delta\dot{f} = 1.76 \times 10^{-9}$ Hz s^{-1}). The total number of explored points in the source parameter space is given by $N_{\rm tot} = N_f \times N_{\rm sky} \times N_{\rm sd}$, see [2] for the details. We have $N_{\rm tot} \simeq 2.1 \times 10^{13}$ for C6 and $N_{\rm tot} \simeq 5.3 \times 10^{12}$ for C7. In the case of the optimal analysis, where $T_{\rm FFT} = T_{\rm obs}$, we would have $N_{\rm tot}^{\rm (opt)} \simeq 4.1 \times 10^{25}$ for C6 and $N_{\rm tot}^{\rm (opt)} \simeq 3.5 \times 10^{22}$ for C7. Then, we have a huge reduction in the dimension of the parameter space.

The input of the Hough transform is the peak map and for each search frequency and spin-down value produces a Hough map, i.e. a histogram in the sky position. Cells in the sky with a high count number identify potentially interesting points in the parameter space and are selected for the next steps of the analysis. More precisely, we select candidates *of the first order* on each Hough map putting a threshold on the critical ratio (CR), which is a function of the sky cell defined as $\mathrm{CR} = \frac{n-\mu}{\sigma}$ where n is the count number in the given cell, μ and σ are the average count number and standard deviation of the map. The choice of this threshold is done as a compromise between the needs to limit the sensitivity loss and to have a manageable number of candidates *of the first order*. In this analysis we have chosen $\mathrm{CR}_{\rm thr} = 3.8$. The resulting number of candidates *of the first order* is $N_{\rm cand} = 922,999,536$ for C6 and $N_{\rm cand} = 319,201,742$ for C7[16]. The corresponding false alarm probabilities, given by $P_{\rm fa} = N_{\rm cand}/N_{\rm tot}$, are $P_{\rm fa} = 1.23 \times 10^{-4}$ for C6 and $P_{\rm fa} = 1.70 \times 10^{-4}$ for C7. The theoretical values, that we would expect in the case of ideal noise and long observation time, are lower. The false alarm probability would be $P_{\rm fa}^{\rm (th)} = 7.2 \times 10^{-5}$ with a corresponding number of candidates *of the first order* $N_{\rm cand}^{\rm (th)} \simeq 5.4 \times 10^8$ for C6 and $N_{\rm cand}^{\rm (th)} \simeq 1.4 \times 10^8$ for C7. For ideal noise, the distribution of the count number n in the Hough maps would be binomial, with a 'success' probability, i.e. the probability of selecting a time–frequency peak at a given time, $p \simeq 0.076$ (using the threshold $\theta = 2.5$ in the selection of peaks). In figure 3, we have plotted the CR distributions found in C6 (left) and in C7 (right) versus the theoretical one. The

[14] Candidates found in the Hough transform step are said *of the first order* to distinguish them from the candidate sources found at the end of the hierarchical procedure.

[15] A more refined *cleaning* procedure is being developed now and will be applied to future analyses.

[16] The Hough transform stage has been performed on the INFN Production grid, http://grid-it.cnaf.infn.it.

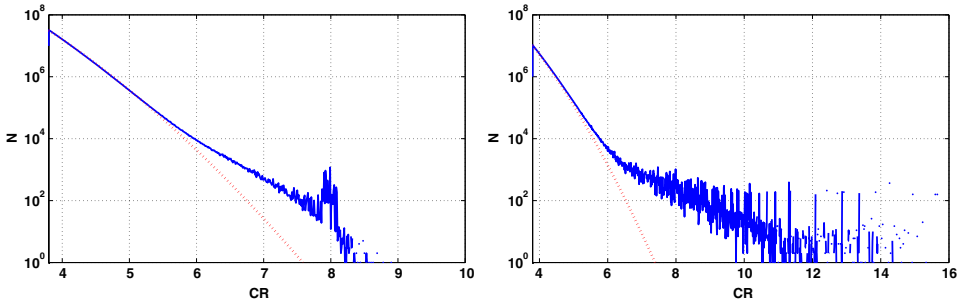

Figure 3. Distribution of the CR for C6 (left) and C7 (right) candidates *of the first order*. The dashed line is the theoretical distribution. The agreement with the theory is very good at low values of CR, while a large deviation appears at high CR for both data sets.

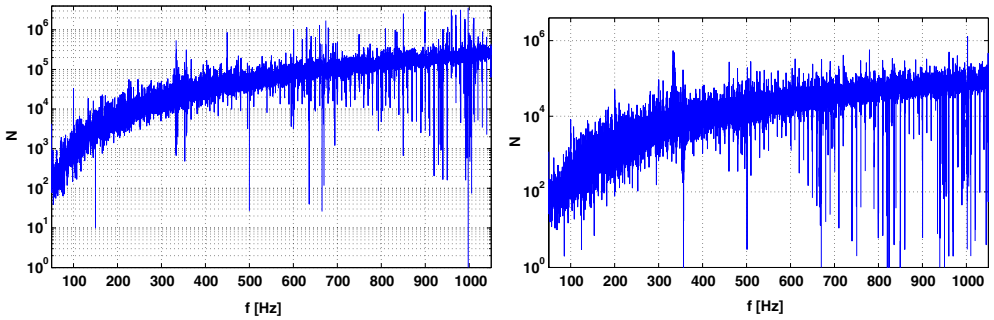

Figure 4. Frequency distribution of candidates *of the first order* with null spin-down for C6 (left) and C7 (right).

deviation of the actual distribution is clearly visible, with respect to the theory, at high values of CR. This is a clear indication of the many disturbances still present in the data.

The presence of disturbances in the data can also be seen looking at the frequency distribution of candidates *of the first order*. This is shown in figure 4 for candidates with no spin-down. We have found a similar behaviour for all the spin-down values. Candidate excess appears at many frequencies. Some excesses have been identified to be due to known noise lines [7], like the first mode-cleaner violin mode around 330 Hz. In most cases the excess is due to unknown disturbances. The increase in the number of candidates with frequency is in agreement with the quadratic increase of the sky resolution with the frequency, see section 3.

Disturbances obviously also appear in the sky distribution of candidates *of the first order*. Also in the quiet frequency bands, however, many candidates are distributed in 'bumps' and 'strips' in the sky. This is the result of the short observation time, so that the Doppler effect is not effective enough in discriminating different directions in the sky, and, especially for candidates at low latitude, of the use of the ecliptical coordinates and of the fact that the detector velocity vector has a large component along the ecliptic [8]. We expect these effects will become less important analysing longer data stretch and using the adaptive Hough transform which, taking into account the detector radiation pattern, breaks the symmetry with respect to the ecliptic.

2.6. Coincidences among candidates of different data sets

We make coincidences among the candidates *of the first order* found into two or more data sets, not necessarily belonging to the same detector, in order to reduce the false alarm probability

and the computational load of the following coherent step of the analysis. Two candidates are coincident if their parameters are within a given coincidence window. Here we have done coincidences among the candidates *of the first order* found in C6 and C7 data. Using a coincidence window width (in number of bins) $\Delta f = 2$ (i.e. 0.019 Hz); $\Delta \dot{f} = 1$ (i.e. 8.12×10^{-10} Hz s^{-1} for C6 and 3.52×10^{-9} Hz s^{-1} for C7); $\Delta\lambda = 2$; $\Delta\beta = 2$,[17] we have found 2700 232 coincident candidates corresponding to a false alarm rate reduced to 2.2×10^{-7}, about three orders of magnitude lower than in the original candidate sets.

2.7. Coherent step

On the coincident candidates, the coherent follow-up has to be applied. It consists of correcting data for the Doppler shift and spin-down using candidate parameters and it is based on the so-called analytical signal [9]. In this way, longer FFTs can be computed, in which the power of a signal would be all confined within a frequency bin. The false alarm probability is reduced to a negligibly small value with this step. If some candidates still survive they can be checked by analysing a longer data set or making coincidences with candidates found in other data sets. In the analysis described in this paper we have not performed the coherent step.

3. Search sensitivity

The sensitivity of our hierarchical method can be computed starting from the optimal 'nominal' sensitivity (i.e. with SNR = 1), which is $h^{(\mathrm{opt})}_{\mathrm{SNR}=1} = \tilde{h} \times \sqrt{\frac{2}{T_{\mathrm{obs}}}}$ where $\tilde{h}$ is the noise spectral density, taking into account various loss factors. In the case of an incoherent method in which data are divided in chunks of duration T_{FFT}, there is a loss factor

$$\sqrt[4]{\frac{2T_{\mathrm{obs}}}{T_{\mathrm{FFT}}}} = \sqrt[4]{N_{\mathrm{FFT}}}$$

where the factor 2 takes into account the overlapping of FFTs. A further reduction in sensitivity comes from the selection of candidates *of the first order* with $\mathrm{CR} > CR_{\mathrm{thr}}$ ($\mathrm{CR}_{\mathrm{thr}} = 3.8$ in our case), given by $\sqrt{CR_{\mathrm{thr}}}$. Finally, a factor $\sim$1.12 must be considered due to the loss of our method, based on the peak map, with respect to the 'classical' incoherent method (Radon transform *aka* stack-slide method) where the full spectral information is used.

From what has been told, we can express the amplitude of the smallest signal that would produce a candidate *of the first order* in the Hough map, at 95% confidence level, as

$$h_{\mathrm{min}} \simeq 2.2 \times \tilde{h} \sqrt[4]{\frac{4\mathrm{CR}^2_{\mathrm{thr}}}{T_{\mathrm{obs}} T_{\mathrm{FFT}}}}. \tag{1}$$

It can be shown that there is an overall loss factor with respect to the optimal analysis, after selection of the same number of candidates, of 2.42 for C6 and 1.84 for C7. We can take into account the noise non-stationarity, i.e. the fact that $\tilde{h}$ is not constant in time, replacing it with an *effective* noise, defined as that stationary noise that would give the same average sensitivity over the same observation window. It can be shown that we can express the *effective* noise as

$$\tilde{h}^{\mathrm{eff}} = \left(\frac{1}{N_{\mathrm{FFT}}} \sum_{i=1}^{N_{\mathrm{FFT}}} \frac{1}{\tilde{h}_i^2} \right)^{-1/2} \tag{2}$$

where $\tilde{h}_i$ is the spectral noise density for the ith periodogram. In figure 5, we have plotted the *effective* sensitivity for C6 and C7, computed from equations (1) and (2), corresponding to a confidence level of 95%.

[17] The value of the coincidence window in dimensional units depends on the frequency for the sky coordinates.

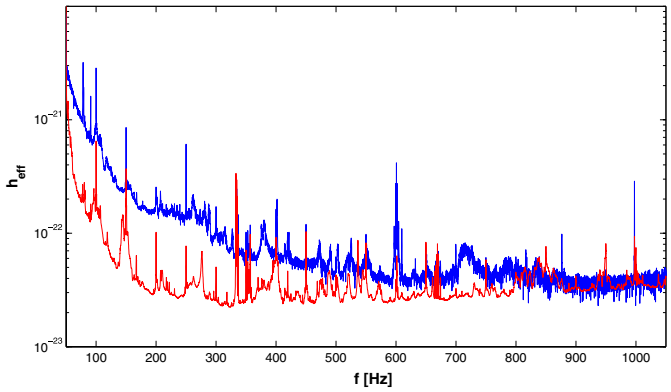

Figure 5. *Effective* sensitivity, at 95% confidence level, for C6 (blue—dark grey in the print version) and C7 (red—light grey in the print version).

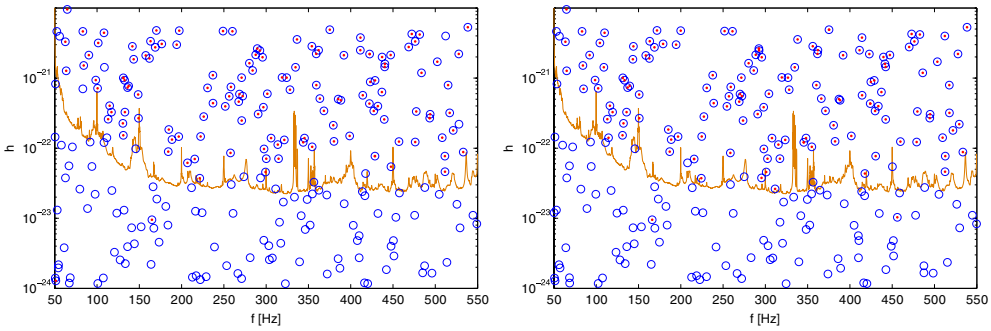

Figure 6. Left: gravitational wave strain amplitude of the injected signals (circles) and the detected ones (dots) for C7 data. Right: gravitational wave strain amplitude of the injected signals (circles) and the detected ones (dots) for 'dilated' C7 data. The continuous line is the *effective* sensitivity at 95% confidence level.

4. Injection of simulated signals

In order to study the detection efficiency of our pipeline and the accuracy in source parameter estimation we have injected 244 simulated signals in C7 data. Signals uniformly span the frequency range between 50 Hz and 550 Hz, spin-down smaller than 1.66×10^{-8} Hz s^{-1}, a dimensional amplitude at the detector between 10^{-24} and 10^{-20} and correspond to sources uniformly distributed in the sky. The injected signals are searched for by analysing C7 data (after signals injection) and making coincidences between the found candidates *of the first order* and the list of signals. Concerning the coincidence window, we have chosen (*a posteriori*) the following values: $\Delta f = 2$, $\Delta \dot{f} = 1$, $\Delta\lambda = 3$, $\Delta\beta = 6$. A wider window for the sky position, with respect to that used for coincidences among C6 and C7 candidates, has been chosen to guarantee a good detection efficiency, see below. In figure 6 (left), we have plotted the amplitude of injected signals as a function of their frequency (blue circles) and the detected ones, whenever there is a candidate coincident with one of the signals (red dots). The continuous curve is the *effective* sensitivity of Virgo for C7, at 95% confidence level. From the figure we see that few signals are undetected, even if with amplitude well above the

effective sensitivity. This is connected to the short observation time, as already discussed in section 2, which implies that the coincidence window, for the sky coordinates, is not large enough. To check if a longer observation time would indeed improve the detection efficiency we have produced a new set of C7 data (plus injections) dilated by a factor of 80 (i.e. the time distance between two consecutive FFTs is increased by 80, their length remaining the same) and repeated the analysis. The result is shown in figure 6 (right): now basically all signals above the *effective* sensitivity are detected, using the same coincidence window as before. Using a smaller coincidence window we would also lose some signals in this case.

5. Conclusions

We have a well established procedure for going from the data to source candidates. We have described in this paper its application to C6 and C7 Virgo data. An important step consists of making coincidences between the candidates *of the first order* found in two or more data sets, in order to reduce the false alarm probability. The coherent follow-up of the coincident candidates reduces the false alarm probability to negligibly small values.

To check detection efficiency and accuracy in source parameter estimation, we have also analysed C7 data after the injection of simulated signals. We have seen that the detection efficiency is larger if data cover a larger time interval, because in this case the Doppler effect is effective in discriminating different locations in the sky. We have found a poorer accuracy for sources at low latitude, due to the symmetry of our problem. This implies that there is a need to increase the coincidence window. However, we expect to have a better accuracy using the adaptive Hough transform which breaks the symmetry with respect to the ecliptic. In general, the detection efficiency is in very good agreement with what we expect on the basis of the data and the parameters we use.

More systematic injections will allow us to establish upper limits to the amplitude of periodic gravitational signals from unknown sources in the Virgo data.

References

[1] Palomba C 2005 *Mon. Not. R. Astron. Soc.* **359** 1050
[2] Frasca S, Astone P and Palomba C 2005 *Class. Quantum Grav.* **22** S1013
[3] Astone P, Frasca S and Palomba C 2007 *Proc. 11th Marcel Grossmann Meeting* (Singapore: World Scientific) at press
[4] Astone P, Frasca S and Palomba C 2005 *Class. Quantum Grav.* **22** S1197
[5] Krishnan B, Sintes A M, Papa M A, Schutz B F, Frasca S and Palomba C 2004 *Phys. Rev.* D **70** 082001
[6] Sintes A M *et al* 2006 *J. Phys.: Conf. Ser.* **39** 36
[7] Acernese F *et al* 2007 Analysis of noise lines in the Virgo C7 data *Class. Quantum Grav.* **24** S433
[8] Palomba C, Astone P and Frasca S 2005 *Class. Quantum Grav.* **22** S1255
[9] Astone P *et al* 2002 *Phys. Rev.* D **65** 022001